Hamiltonian Gust Load Alleviation Control with Adaptive Gust Estimation: Analysis and Wind Tunnel Test Correlation

Christopher J. Forte*
KBR Wyle, Inc., Moffett Field, CA 94035

Nhan T. Nguyen†
NASA Ames Research Center, Moffett Field, CA 94035

John K. Berg‡
University of Washington, Seattle, Washington, 98195

Kuang-Ying Ting§
University of Washington, Seattle, Washington, 98195

Eli Livne¶
University of Washington, Seattle, Washington, 98195

This paper presents the design and experimental validation of a Hamiltonian controller for gust load alleviation (GLA) on a flexible wing wind tunnel model. The control design incorporates practical implementation considerations, including low-pass filtering to prevent excitation of high-frequency structural modes, LQR stabilization of actuator dynamics, and state and gust estimation via an extended-state Kalman filter. The Hamiltonian GLA controller is implemented on the Large Flexible Wing (LFW) test article, an 8.36 aspect ratio Generic Transport Model employing the VCCTEF concept, in active control experiments conducted at the University of Washington's 12 ft by 8 ft Kirsten Wind Tunnel. Experimental results demonstrate substantial attenuation of structural response due to gust disturbances. Additionally, an adaptive gust estimation scheme is proposed, derived from the structural dynamics equations, to improve robustness to uncertainty in gust frequency, motivated by discrepancies observed in wind tunnel gust measurements.

I. Introduction

The aircraft industry has been responding to the demand for increased efficiency by redesigning modern aircraft. New designs include energy-efficient engines and the redesign of airframes to be aerodynamically and structurally more efficient. A major consideration for improving energy-efficiency is reducing the airframe operational empty weight by employing advanced lightweight composite materials. However, these lightweight materials can provide less structural rigidity while still maintaining sufficient load carrying capacity. The increase in wing aspect ratio exacerbates this problem as the wing twist under load can be substantial. Aeroelastic interactions with aerodynamic forces can adversely affect the aerodynamic performance as flexibility increases[1]. Structures may also be more susceptible to these aeroelastic interactions such as gust with increased structural flexibility. One approach to mitigating gust disturbances is the use of an active control system [2–6].

An active control wind tunnel experiment was conducted at the University of Washington Aerodynamic Laboratory's 12 ft × 8 ft Kirsten Wind Tunnel (KWT). The test article is the Large Flexible Wing (LFW) model which is built for active aeroelastic testing seen in Fig. 1. The LFW is a fourth iteration VCCTEF[7, 8] concept wing that is based on the NASA/Boeing generic transport model (GTM) with an aspect ratio of 8.36 and span of 85 inches. Previous studies include VCCTEF/GTM concept wind tunnel models [9–12], some of which involved active control experiments [13, 14].

*Aerospace Engineer, Intelligent System Division, Member AIAA.
†Senior Research Scientist, Technical Group Lead, Intelligent Systems Division, Associate Fellow AIAA.
‡Ph.D. Candidate, William E. Boeing Department of Aeronautics and Astronautics; jberg26@uw.edu. Student Member AIAA.
§Ph.D. Student, William E. Boeing Department of Aeronautics and Astronautics; kyting@us.edu. Student Member AIAA.
¶Boeing Endowed Professor, William E. Boeing Department of Aeronautics and Astronautics; mmor@uw.edu. Fellow AIAA.

This iteration includes a major redesign of the sensing, actuation, and control systems, enabling reliable and repeatable aeroelastic testing [15].

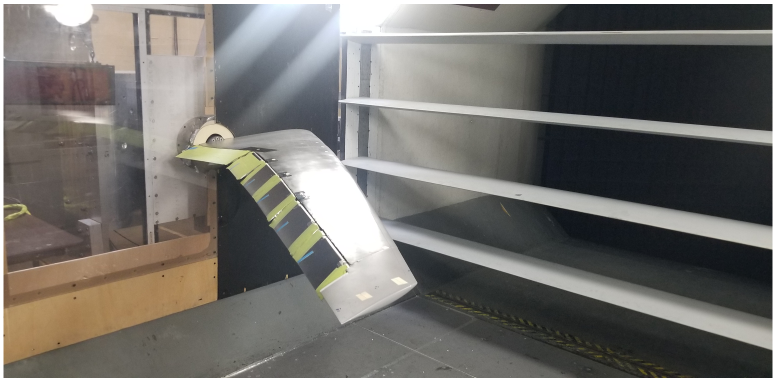

Fig. 1 Large Flexible Wing In Kirsten Wind Tunnel Test Section

The LFW has six control surfaces distributed along the trailing edge of the wing seen in Fig. 2. The article is also equipped with 10 accelerometers and 2 strain gages that can be utilized for control law implementation [16]. The Kirsten Wind Tunnel is equipped with a gust generation system (GGS). The GGS uses gust vanes upstream of the model to generate gust disturbances. The GGS can produce both sinusoidal and discrete gusts, providing the opportunity to test gust load alleviation (GLA) control strategies on the LFW [15, 17].

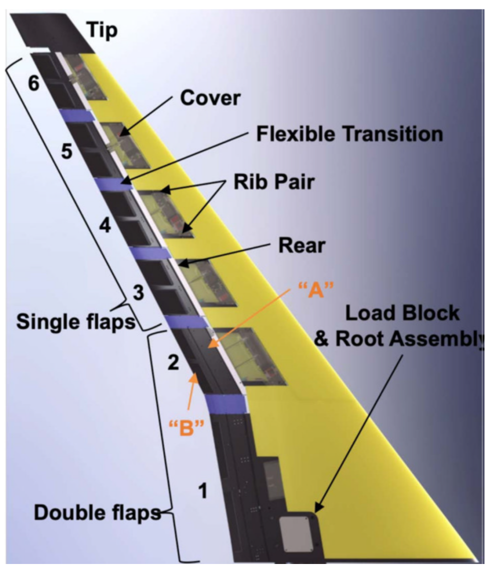

Fig. 2 Large Flexible Wing Control Surface Layout

Distributed control theory for distributed Lagrangian infinite-dimensional systems is introduced by Nguyen[18–23]. This paper details the practical implementation of distributed Hamiltonian control for the LFW. The distributed Lagrangian system is defined and related to the structural dynamics of the LFW aeroservolastic (ASE) model[16]. Hamiltonian control gains are computed and, together with Kalman filtering for state and gust estimation, are tested in an active control experiment on the LFW. An adaptive gust estimator is also proposed to improve gust estimation, derived from the structural dynamics equation.

II. GLA Controller Design

The state-space model of the large flexible wing is given by:

$$\begin{bmatrix} \dot{x}_f(t) \\ \dot{x}_b(t) \\ \dot{x}_a(t) \\ \dot{x}_g(t) \end{bmatrix} = \begin{bmatrix} A_f & A_{fb} & A_{fa} & A_{fg} \\ 0 & A_b & A_{ba} & A_{bg} \\ 0 & 0 & A_a & 0 \\ 0 & 0 & 0 & A_g \end{bmatrix} \begin{bmatrix} x_f(t) \\ x_b(t) \\ x_a(t) \\ x_g(t) \end{bmatrix} + \begin{bmatrix} B_f & E_f \\ B_b & E_b \\ B_a & 0 \\ 0 & E_g \end{bmatrix} \begin{bmatrix} u(t) \\ g(t) \end{bmatrix} \tag{1}$$

where x_f is the anti-aliasing filter state vector, x_g is the gust state vector, u is the control input and g is the gust input. The first bending mode is represented by x_b, which contains the generalized displacement $q(t)$ and velocity $\dot{q}(t)$:

$$x_b(t) = \begin{bmatrix} q(t) \\ \dot{q}(t) \end{bmatrix} \tag{2}$$

The control inputs are partitioned such that u_b corresponds to Hamiltonian control, while u_r represents the remaining control surfaces:

$$u(t) = \begin{bmatrix} u_r(t) \\ u_b(t) \end{bmatrix} \tag{3}$$

$$u_r(t) = Eu(t) \tag{4}$$

$$u_b(t) = eu(t) \tag{5}$$

The structural state dynamics can then be written as:

$$\dot{x}_b(t) = A_b x_b(t) + A_{ba} x_a(t) + A_{bg} x_g(t) + B_{b_b} u_b(t) + B_{b_r} u_r(t) + E_b g(t) \tag{6}$$

The structural dynamics can be expressed in terms of generalized displacement and velocity as:

$$\begin{bmatrix} \dot{q}(t) \\ \ddot{q}(t) \end{bmatrix} = \begin{bmatrix} 0 & I \\ -M^{-1}K & -M^{-1}C \end{bmatrix} \begin{bmatrix} q(t) \\ \dot{q}(t) \end{bmatrix} + \begin{bmatrix} 0 \\ M^{-1}[a_a x_a(t) + a_g x_g(t) + b_r u_r(t) + b_b u_b(t) + e_b g(t)] \end{bmatrix} \tag{7}$$

where M is the generalized mass, K is the generalized stiffness, and C is the damping. The structural dynamics equation is written as:

$$M\ddot{q}(t) + C\dot{q}(t) + Kq(t) = a_a x_a(t) + a_g x_g(t) + b_r u_r(t) + b_b u_b(t) + e_b g(t) \tag{8}$$

These dynamics are then written as a distributed Lagrangian system

$$\frac{\partial^2 w(x,t)}{\partial t^2} + Lw(x,t) = m^{-1}(x)Q(x,t) \tag{9}$$

where $w(x,t) = \phi(x)q(t)$ is the physical displacement along the elastic axis defined by the coordinate x, $m(x)$ is the distributed mass, L is a linear differential operator representing the stiffness, and $Q(x,t)$ is the non-conservative force. $\phi(x)$ is the generalized mode shape along the elastic axis.

The non-conservative force $Q(x,t)$ is modeled as:

$$Q(x,t) = -m(x)c\frac{\partial w(x,t)}{\partial t} + Q_a(x)x_a(t) + Q_{x_g}(x)x_g(t) + Q_{u_r}(x)u_r(t) + Q_{u_b}(x)u_b(t) + Q_g(x)g(t) \tag{10}$$

Then,

$$a_a = \langle \phi(x), Q_a(x) \rangle \tag{11}$$

$$a_g = \langle \phi(x), Q_{x_g}(x) \rangle \tag{12}$$

$$b_r = \langle \phi(x), Q_{u_r}(x) \rangle \tag{13}$$

$$b_b = \langle \phi(x), Q_{u_b}(x) \rangle \tag{14}$$

$$e_g = \langle \phi(x), Q_g(x) \rangle \tag{15}$$

The mass-weighted inner product is defined as:

$$\langle \xi, v \rangle = \int_{\Omega} \phi(x) m(x) v dx \tag{16}$$

The generalized mass, damping, and stiffness are obtained from,

$$M = \langle \phi(x), \phi(x) \rangle \tag{17}$$

$$C = \langle \phi(x), c\phi(x) \rangle \tag{18}$$

$$K = \langle \phi(x), L(x)\phi(x) \rangle \tag{19}$$

The Hamiltonian is defined as:

$$H = \frac{1}{2}\left\langle \frac{\partial w(x,t)}{\partial t}, \frac{\partial w(x,t)}{\partial t} \right\rangle + \frac{1}{2}\langle w(x,t), L(x)w(x,t) \rangle > 0 \tag{20}$$

The time derivative of the Hamiltonian is given by:

$$\dot{H} = \left\langle \frac{\partial w(x,t)}{\partial t}, \frac{\partial^2 w(x,t)}{\partial t^2} + L(x)w(x,t) \right\rangle \tag{21}$$

$$\begin{aligned} \dot{H} = &\left\langle \frac{\partial w(x,t)}{\partial t},\ -c\frac{\partial w(x,t)}{\partial t} + m^{-1}(x)\left[Q_a(x)x_a(t) + Q_{x_g}(x)x_g(t) + Q_{u_r}(x)u_r(t) + Q_g(x)g(t)\right] \right\rangle \\ &+ \left\langle \phi(x),\ m^{-1}(x)Q_{u_b}u_b(t) \right\rangle \end{aligned} \tag{22}$$

For dissipative control, the Hamiltonian derivative is enforced to satisfy:

$$\dot{H} = -\left\langle \frac{\partial w(x,t)}{\partial t}, (c+\alpha)\frac{\partial w(x,t)}{\partial t} \right\rangle \leq 0 \tag{23}$$

Here, $c + \alpha > 0$ represents the effective closed-loop damping. The variable α is chosen such that the damping ratio $\zeta = \frac{1}{\sqrt{2}}$:

$$C + \alpha = \sqrt{2M^{-1}K} \tag{24}$$

Hamiltonian control is computed using the pseudo-inverse method:

$$\begin{aligned} u_b(t) = -b_b^T(b_b b_b^T)^{-1}\Bigg\langle \phi(x),\ -c\frac{\partial w(x,t)}{\partial t} + m^{-1}(x)\Big[Q_a(x)x_a(t) + Q_{x_g}x_g(t) \\ + Q_{u_r}u_r(t) + Q_g(x)g(t)\Big] + \alpha\frac{\partial w(x,t)}{\partial t} \Bigg\rangle \end{aligned} \tag{25}$$

Substituting the expressions into Eq. 25 yields:

$$u_b(t) = -b_b^T(b_b b_b^T)^{-1}(a_a x_a(t) + a_g x_g(t) + b_r u_r(t) + e_b g(t) + \alpha\dot{q}(t)) \tag{26}$$

$$u_b(t) = -k_{x_a}x_a(t) - k_{x_g}x_g(t) - k_{u_r}u_r(t) - k_g g(t) - k_{x_b}x_b(t) \tag{27}$$

The closed loop system becomes

$$\dot{\bar{x}}(t) = \bar{A}\bar{x}(t) + \bar{B}\begin{bmatrix} u_r(t) \\ g(t) \end{bmatrix} \tag{28}$$

where

$$\bar{x}(t) = \begin{bmatrix} x_f(t) \\ x_b(t) \\ x_a(t) \\ x_g(t) \end{bmatrix} \tag{29}$$

$$\bar{A} = \begin{bmatrix} A_f & A_{fb} - B_f e^T k_{x_b} & A_{fa} - B_f e^T k_{x_a} & A_{fg} - B_f e^T k_{x_g} \\ 0 & A_b^* & 0 & 0 \\ 0 & -B_a e^T k_{x_b} & A_a - B_a e^T k_{x_a} & -B_a e^T k_{x_g} \\ 0 & 0 & 0 & A_g \end{bmatrix} \tag{30}$$

$$\bar{B} = \begin{bmatrix} B_f E^T - B_f e^T k_{u_r} & E_f - B_f e^T k_g \\ 0 & 0 \\ B_a E^T - B_a e^T k_{u_r} & -B_a e^T k_g \\ 0 & e_g \end{bmatrix} \tag{31}$$

In this implementation, Hamiltonian control stabilizes the structural dynamics but destabilizes the actuator dynamics. As a result, the control commands grow exponentially even though the structural states are stable. Therefore, the remaining control input u_r is designed to stabilize the actuator dynamics.

The actuator plant matrices are

$$A_a^* = A_a - B_a e^T k_{x_a} \tag{32}$$

$$B_a^* = B_a E^T - B_a e^T k_{u_r} \tag{33}$$

The pair $(A_a^* B_a^*)$ is controllable, so the control command u_r that stabilizes the actuator dynamics is given by:

$$u_r = -K_{x_a} x_a \tag{34}$$

where the gain K_{x_a} is computed using a Linear Quadratic Regulator (LQR).

An additional consideration in the controller design is filtering the control signal. The LFW state-space model includes only the first structural mode, and its frequency response matches experimental data up to approximately 5 Hz. Beyond 5 Hz, the model is no longer valid. Therefore, a low-pass Butterworth filter with a 5 Hz cutoff is applied to the control signal to prevent excitation of higher-frequency modes. The low-pass filter also introduces a phase delay in the control command. An LQI controller is then used to track the control command.

In order to estimate the gust, an extended-state Kalman filter is used. The system is considered with consolidated states, defined as:

$$x(t) = \begin{bmatrix} x_f(t) \\ x_b(t) \\ x_a(t) \\ x_g(t) \end{bmatrix} \tag{35}$$

The consolidated system, also separating the gust, becomes

$$\dot{x}(t) = Ax(t) + Bu(t) + Eg(t) \tag{36}$$

$$y(t) = Cx(t) + Fg(t) \tag{37}$$

The gust disturbance is sinusoidal with frequency ω.

$$g(t) = \sin(\omega t + \phi) \tag{38}$$

The gust dynamics are represented in state-space form as:

$$\dot{x}_w(t) = A_w x_w(t) \tag{39}$$

where

$$x_w(t) = \begin{bmatrix} g(t) \\ \dot{g}(t) \end{bmatrix} \tag{40}$$

$$A_w = \begin{bmatrix} 0 & 1 \\ -\omega^2 & 0 \end{bmatrix} \tag{41}$$

$$g(t) = C_w x_w(t) \tag{42}$$

where

$$C_w = \begin{bmatrix} 1 & 0 \end{bmatrix} \tag{43}$$

The system in (36)–(37) is then extended to include $x_w(t)$, resulting in:

$$\dot{x}_e(t) = A_e x_e(t) + B_e u(t) \tag{44}$$

$$y(t) = C_e x_e(t) \tag{45}$$

where,

$$x_e(t) = \begin{bmatrix} x(t) \\ x_w(t) \end{bmatrix} \tag{46}$$

$$A_e = \begin{bmatrix} A & EC_w \\ 0 & A_w \end{bmatrix} \tag{47}$$

$$B_e = \begin{bmatrix} B \\ 0 \end{bmatrix} \tag{48}$$

$$C_e = \begin{bmatrix} C & FC_w \end{bmatrix} \tag{49}$$

A Kalman filter is then computed for the extended system to estimate the state and disturbance. The extended-state Kalman filter is given by:

$$\dot{\hat{x}}_e(t) = A_e \hat{x}_e(t) + B_e u(t) + L(y(t) - C_e \hat{x}_e(t)) \tag{50}$$

The overall control architecture is illustrated in Fig. 3. Sensor measurements and the LQI control output are fed into the Kalman filter to estimate both the system states and the gust disturbance. Hamiltonian control with stabilizing LQR generates a control command, which is then passed through a low-pass filter to prevent excitation of high-frequency structural modes. The filtered command is tracked by the LQI controller, compensating for the phase delay introduced by the filter. Finally, the LQI output is applied to the test article for actuation and simultaneously provided to the Kalman filter for state and disturbance estimation.

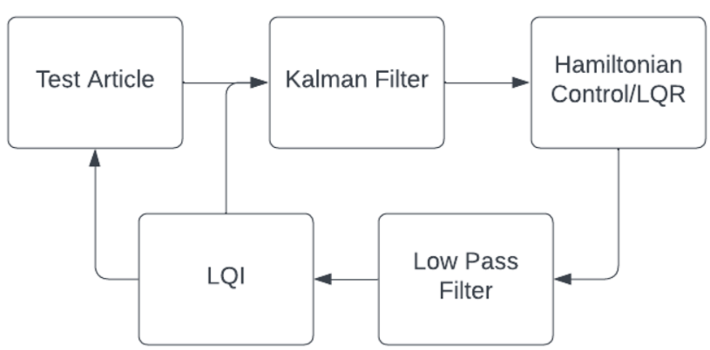

Fig. 3 Controller Diagram

III. Adaptive Disturbance Rejection

A drawback of the extended-state Kalman filter implementation is that it assumes the gust frequency ω is known. If the true gust frequency differs significantly from the frequency used in the Kalman filter design, the estimation performance can degrade. This results in inaccurate gust and state estimates, which can adversely affect controller performance. An adaptive gust rejection strategy can address this issue and improve gust estimation performance when gust frequency is not known with sufficient accuracy.

The Hamiltonian control in (27) is written in terms of gust estimate $\hat{g}(t)$.

$$u_b(t) = -k_{x_a} x_a(t) - k_{x_g} x_g(t) - k_{u_r} u_r(t) - k_g \hat{g}(t) - k_{x_b} x_b(t) \tag{51}$$

The closed-loop structural states system is written as

$$\dot{x}_b(t) = A_b^* x_b(t) + E_b(g(t) - \hat{g}(t)) = A_b^* x_b(t) - E_b \tilde{g}(t) \tag{52}$$

where

$$\tilde{g}(t) = g(t) - \hat{g}(t) \tag{53}$$

$$A_b^* = \begin{bmatrix} 0 & I \\ -M^{-1}K & -M^{-1}(C+\alpha) \end{bmatrix} \tag{54}$$

The following Lyapunov function is chosen.

$$V(t) = x_b^T(t) P x_b(t) + \frac{\tilde{g}^2(t)}{\gamma} \tag{55}$$

where $P > 0$ and $\gamma > 0$ Taking the derivative yields

$$\begin{aligned} \dot{V}(t) &= \dot{x}_b(t) P x_b(t) + x_b^T(t) P \dot{x}_b(t) + 2\frac{\tilde{g}(t)\dot{\tilde{g}}(t)}{\gamma} \\ &= (x_b^T(t) A_b^{*T} - \tilde{g}(t) E_b^T) P x_b(t) + x_b^T(t) P (A_b^* x_b(t) - E_b \tilde{g}(t)) + 2\frac{\tilde{g}(t)\dot{\tilde{g}}(t)}{\gamma} \\ &= x_b^T(t)(A_b^{*T} P + P A_b^*) x_b(t) - 2\tilde{g}(t) E_b^T P x_b(t) + 2\frac{\tilde{g}(t)\dot{\tilde{g}}(t)}{\gamma} \end{aligned} \tag{56}$$

Let P be the solution of the Lyapunov equation

$$A_b^{*T} P + P A_b^* = -Q < 0 \tag{57}$$

$\dot{\tilde{g}}(t)$ is chosen as follows

$$\dot{\tilde{g}}(t) = \gamma E_b^T P x_b(t) \tag{58}$$

Then,

$$\dot{V}(t) = -x_b^T(t) Q x_b(t) \le 0 \tag{59}$$

The adaptive gust estimation is

$$\dot{\tilde{g}}(t) = \dot{\hat{g}}(t) - \dot{g}(t) = \gamma E_b^T P x_b(t) \tag{60}$$

which yields

$$\dot{\hat{g}}(t) = \gamma E_b^T P x_b(t) - \dot{g}(t) \tag{61}$$

The problem is that $\dot{g}(t)$ is not known. However, $\dot{g}(t)$ can be obtained from the structural state model. The structural state model is written as

$$\begin{aligned} \ddot{q}(t) &= \begin{bmatrix} 0 & 1 \end{bmatrix} \dot{x}_b(t) \\ &= \begin{bmatrix} 0 & 1 \end{bmatrix} A_b^* x_b(t) + \begin{bmatrix} 0 & 1 \end{bmatrix} E_b g(t) \\ &= a_b^* x_b(t) + e_b g(t) \end{aligned} \tag{62}$$

The equations at the current time and most immediate past are considered

$$\ddot{q}(k) = a_b^* x(k) + e_b g(k) \tag{63}$$

$$\ddot{q}(k-1) = a_b^* x(k-1) + e_b g(k-1) \tag{64}$$

where $t = kT$ and T is the sampling period. Then, $\dot{g}(t)$ can be approximated by a backward difference method as

$$\dot{g}(t) \approx \frac{g(k) - g(k-1)}{T} = \frac{\ddot{q}(k) - \ddot{q}(k-1) - a_b^*[x_b(k) - x_b(k-1)]}{e_b T} \tag{65}$$

Thus, the adaptive gust estimation is obtained in discrete time as

$$\hat{g}(k) = \hat{g}(k-1) + \gamma T E_b^T P x_b(k) - \frac{\ddot{q}(k) - \ddot{q}(k-1) - a_b^*[x_b(k) - x_b(k-1)]}{e_b T} \tag{66}$$

Fig. 4 compares gust estimation using the extended-state Kalman filter (ESKF) and the proposed adaptive estimation scheme. The ESKF is designed assuming a gust frequency of 2.5 Hz, whereas the true gust frequency is 2.25 Hz. As a result, the ESKF fails to accurately track the gust, highlighting the sensitivity of this approach to precise knowledge of the gust frequency. In contrast, the adaptive estimation scheme successfully tracks the gust without prior frequency information. This method relies on $\ddot{q}$ measurements, which are not readily available in practice; therefore, it should be combined with a suitable estimation scheme.

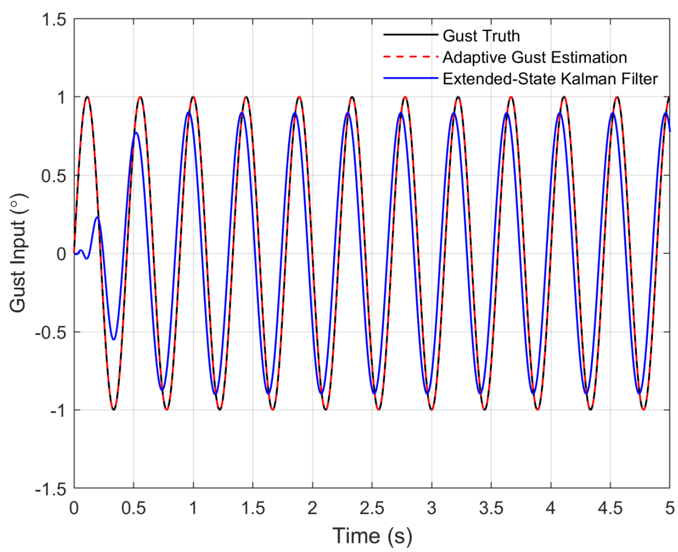

Fig. 4 Gust Estimation Scheme Comparison

IV. Wind Tunnel Test Results

The Hamiltonian GLA controller, as designed in Fig. 3, was implemented on the LFW test article in the 12 ft by 8 ft Kirsten Wind Tunnel. In this configuration, the outermost control surfaces, δ_5 and δ_6, were assigned to the Hamiltonian control, while δ_3 and δ_4 were used for stabilizing LQR. The wind tunnel operated at a dynamic pressure of 8 psf, and the test article was set to a 3° root angle of attack. Gust disturbances were generated using the Gust Generation System (GGS), which was commanded to oscillate at 2.5 Hz with an amplitude of 1°.

It is important to note that the adaptive gust estimation scheme introduced in Section 4 was not implemented during these tests. Its development was motivated by the uncertainty in the actual gust frequency observed during testing, which highlighted the sensitivity of conventional extended-state Kalman filtering to precise frequency knowledge.

Figs. 5 and 6 show accelerometer measurements for test cases with the controller inactive and active. The results demonstrate that the Hamiltonian GLA controller effectively attenuates the response due to the gust disturbance. Figs. 7 and 8 present the corresponding control commands, indicating that the control effort remains well within allowable deflection ranges. Figs. 9 and 10 show the Kalman filter estimates of the sensor outputs, which closely match the actual test article measurements.

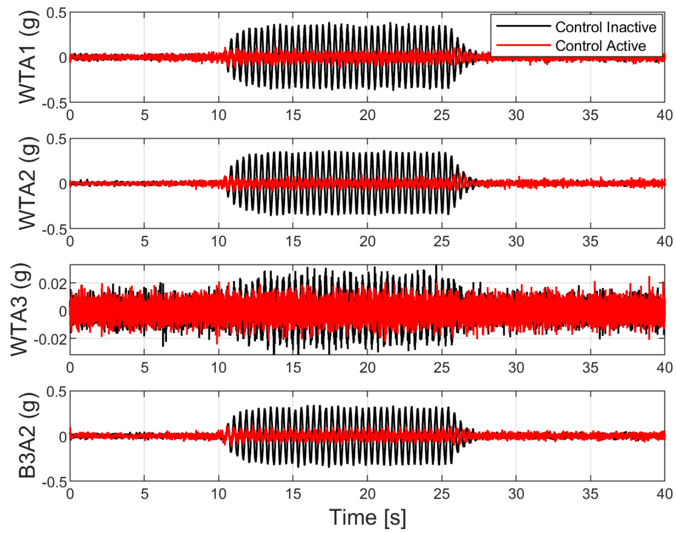

Fig. 5 Test Results: Sensor Output

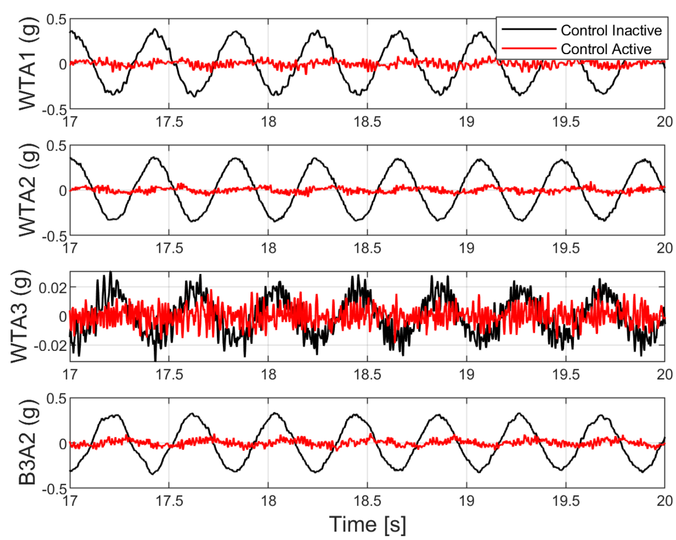

Fig. 6 Test Results: Sensor Output (Zoomed)

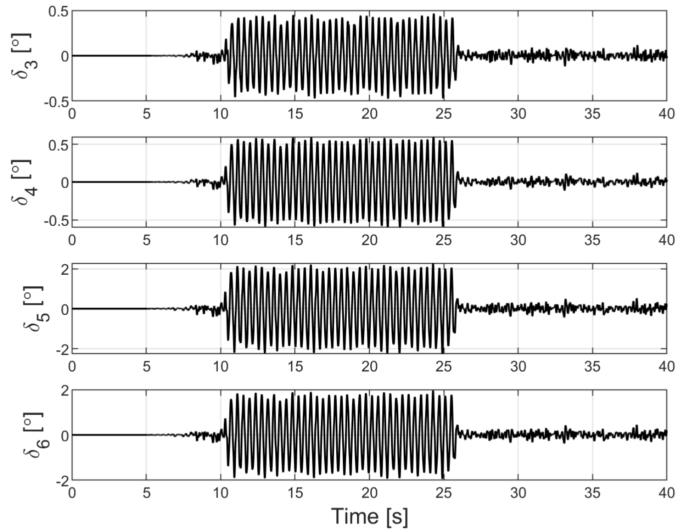

Fig. 7 Test Results: Control Command

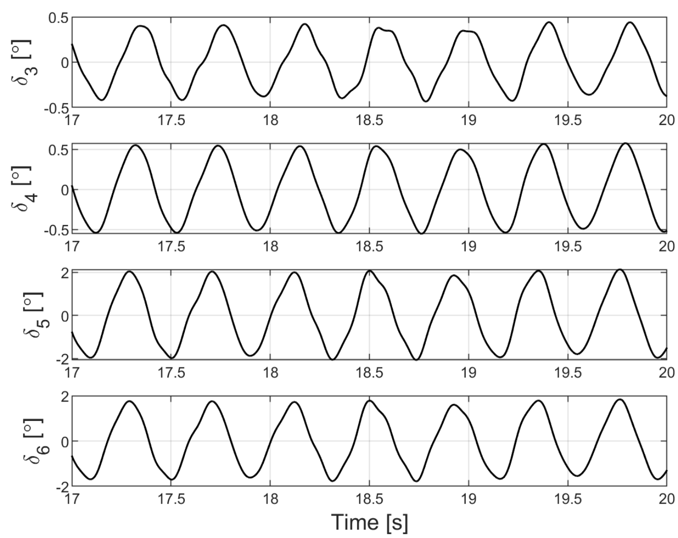

Fig. 8 Test Results: Control Command (Zoomed)

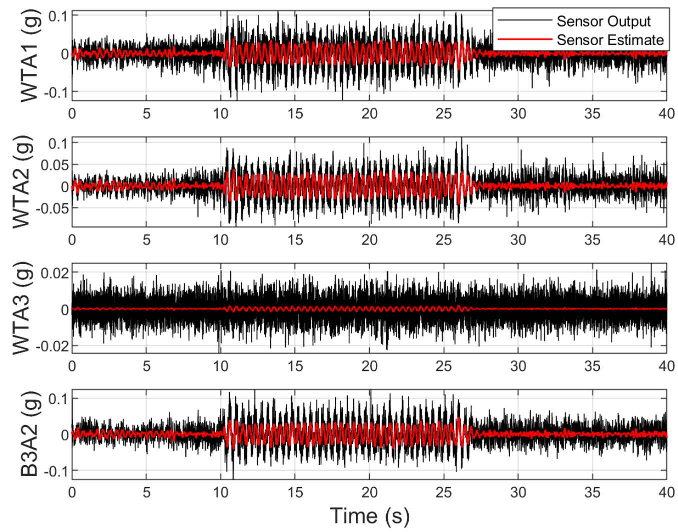

Fig. 9 Test Results: Kalman Filter Sensor Estimation

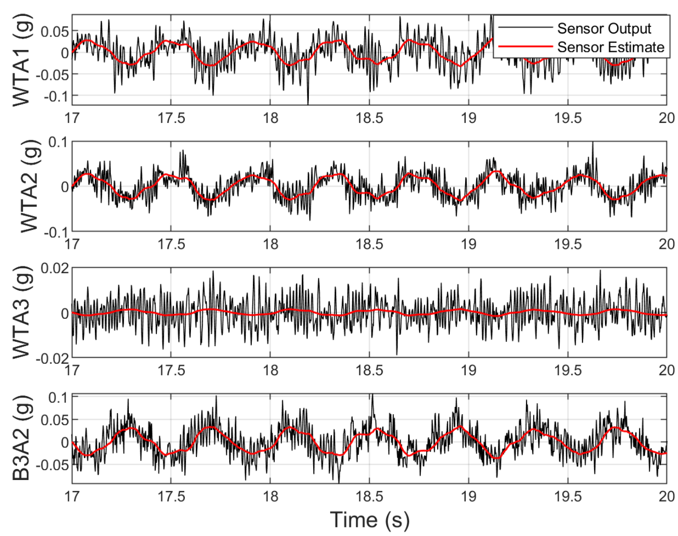

Fig. 10 Test Results: Kalman Filter Sensor Estimation (Zoomed)

Fig. 11 compares the gust estimation from the extended-state Kalman filter to the commanded gust. The initial results show poor tracking due to discrepancies between the commanded and actual GGS actuation. For example, while the GGS was commanded at 2.5 Hz, it oscillated at approximately 2.43 Hz.

To account for this, a corrected gust input, $g(t)$, was generated using the state-space model in Eqs. (36) and (37). The gust was set as a sinusoid at 2.43 Hz, and the amplitude and phase were adjusted until the simulated ASE output matched the sensor measurements from the test article under open-loop conditions. Fig. 12 shows the close agreement between the simulated ASE response to the corrected gust input and the experimental sensor data.

Fig. 13 show the Kalman filter gust estimates during the closed-loop Hamiltonian GLA run compared to the corrected gust input. The results indicate a substantial improvement in gust estimation accuracy after accounting for the actual GGS actuation. These findings further illustrate the motivation for developing the adaptive estimation scheme, which could mitigate the effects of gust frequency uncertainty in future implementations.

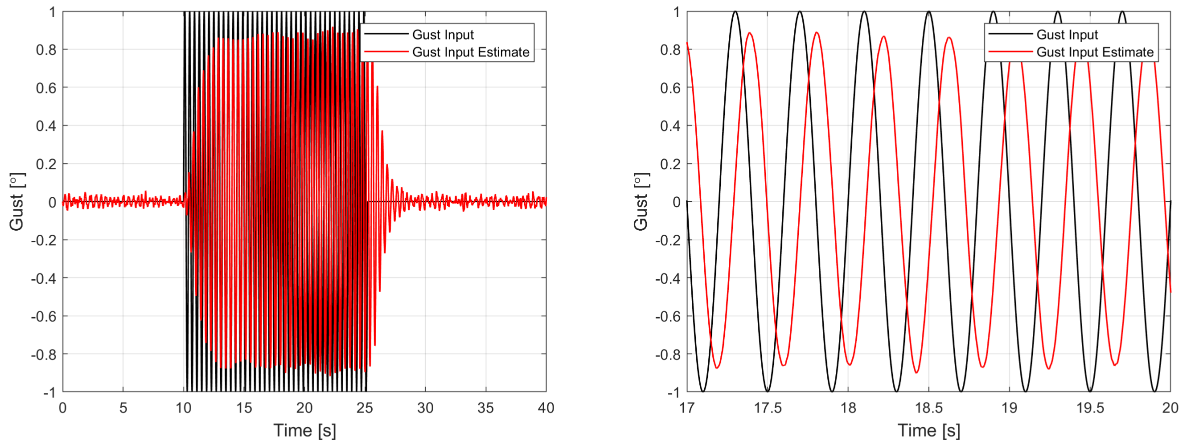

(a) $0 < t < 3$ **(b)** $17 < t < 20$

Fig. 11 Kalman Filter Gust Estimation Compared to Commanded Gust

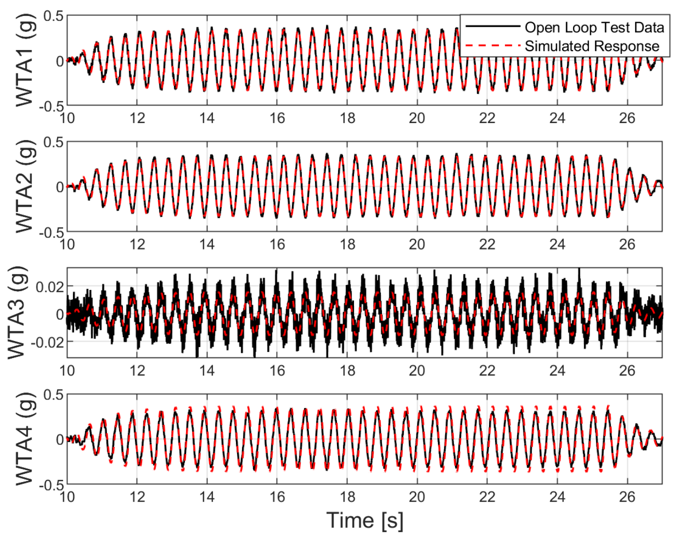

Fig. 12 Simulated Gust Response Matching Test Data

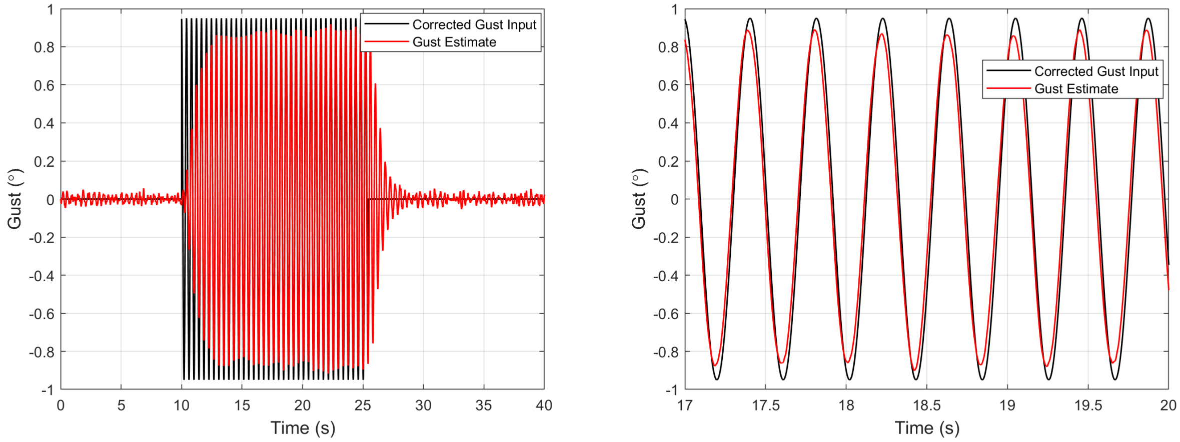

(a) $0 < t < 3$

(b) $17 < t < 20$

Fig. 13 Kalman Filter Gust Estimation with Corrected Gust Input

Conclusions

This paper presents the design and implementation of a Hamiltonian control approach for gust load alleviation, validated through hardware-in-the-loop wind tunnel experiments. The Hamiltonian control law is augmented with an LQR to stabilize the actuator dynamics, while a low-pass filter is employed to prevent excitation of high-frequency structural modes. An LQI controller is incorporated to mitigate the phase effects introduced by the filtering.

A Kalman filter is designed to estimate both the structural states and gust disturbance, providing feedback for the Hamiltonian control. While the Kalman filter requires knowledge of the gust frequency, this work also develops an adaptive gust estimation scheme, derived from Lyapunov analysis of the structural dynamics, which improves robustness to gust frequency uncertainty. It should be noted that the adaptive estimator was not implemented during the wind tunnel tests, but its development was motivated by the observed discrepancies in gust frequency during testing.

The control design is demonstrated on the Large Flexible Wing (LFW) test article, an 8.36 aspect ratio Generic Transport Model geometry utilizing the VCCTEF concept. Active control experiments conducted in the 12 ft by 8 ft Kirsten Wind Tunnel at the University of Washington show that the Hamiltonian controller effectively attenuates the gust-induced structural response. Accelerometer measurements indicate a significant reduction in structural motion when the controller is active, and the Kalman filter accurately estimates both the sensor outputs and the corrected gust input.

Overall, the combination of Hamiltonian control, actuator stabilization, state and gust estimation, and filtering provides a practical and effective framework for gust load alleviation. The proposed adaptive disturbance estimation offers a promising avenue for further improving performance under uncertain or varying gust conditions.

Acknowledgment

The authors gratefully acknowledge the support of NASA's Advanced Air Transport Technology (AATT) project for funding this research. The authors also thank the University of Washington Aerodynamic Laboratory team for their invaluable assistance during the wind tunnel experiments.

References

[1] Nguyen, N., Livne, E., Precup, N., Urnes, J. M., Nelson, C., Ting, E., and Lebofsky, S., "Experimental Investigation of a Flexible Wingwith a Variable Camber Continuous Trailing Edge Flap Design," *AIAA Applied Aerodynamics Conference*, 2014. https://doi.org/https://doi.org/10.2514/6.2014-2441.

[2] Forte, C., and Nguyen, N., “Gust Load Alleviation Control and Gust Estimation for a High Aspect Ratio Wing Wind Tunnel Model,” *AIAA SciTech Forum*, National Harbor, MD, 2023. https://doi.org/https://doi.org/10.2514/6.2023-0881.

[3] Nguyen, N. T., and Tal, E. A., “A Multi-Objective Flight Control Approach for Performance Adaptive Aerolastic Wing,” *AIAA SciTech Forum*, 2015. https://doi.org/https://doi.org/10.2514/6.2015-1843.

[4] Hashemi, K. E., Nguyen, N. T., Drew, M. C., Chaparro, D., and Ting, E., “Performance Optimizing Gust Load Alleviation Control of Flexible Wing Aircraft,” *AIAA SciTech Forum*, 2018. https://doi.org/https://doi.org/10.2514/6.2018-0623.

[5] Ferrier, Y., Nguyen, N. T., Ting, E., Chaparro, D., Wang, X., de Visser, C. C., and Chu, Q. P., “Active Gust Load Alleviation of High-Aspect Ratio Flexible Wing Aircraft,” *AIAA SciTech Forum*, 2018. https://doi.org/https://doi.org/10.2514/6.2018-0620.

[6] Drew, M. C., Hashemi, K. E., Cramer, N. B., and Nguyen, N. T., “Multi-Objective Gust Load Alleviation Control Designs for an Aeroelastic Wind Tunnel Demonstration Wing,” *AIAA SciTech Forum*, 2020. https://doi.org/https://doi.org/10.2514/6.2020-0213.

[7] Nguyen, N., “Elastically Shaped Future Air Vehicle Concept,” *NASA Innovation Fund Award 2010 Report*, 2010.

[8] Nguyen, N., and Urnes, J., “Aeroelastic Modeling of Elastically Shaped Aircraft Concept via Wing Shaping Control for Drag Reduction,” *AIAA Atmospheric Flight Mechanics Conference*, 2012. https://doi.org/https://doi.org/10.2514/6.2012-4642.

[9] Nguyen, N. T., Livne, E., Precup, N., Urnes, J. M., Nelson, C., Ting, E., and Lebofsky, S., “Experimental Investigation of a Flexible Wing with a Variable Camber Continuous Trailing Edge Flap Design,” *AIAA Aviation Forum*, 2014. https://doi.org/https://doi.org/10.2514/6.2014-2441.

[10] Livne, E., Precup, N., and Mor, M., “Design, Construction, and Tests of an Aeroelastic Wind Tunnel Model of a Variable Camber Continuous Trailing Edge Flap (VCCTEF) Concept Wing,” *AIAA Aviation Forum*, 2014. https://doi.org/https://doi.org/10.2514/6.2014-2442.

[11] Precup, N., Mor, M., and Livne, E., “The Design, Construction, and Tests of a Concept Aeroelastic Wind Tunnel Model of a High-Lift Variable Camber Continuous Trailing Edge Flap (HL-VCCTEF) Wing Configuration,” *AIAA SciTech Forum*, 2015. https://doi.org/https://doi.org/10.2514/6.2015-1406.

[12] Nguyen, N. T., Precup, N., Livne, E., Urnes, J. M., Dickey, E., Nelson, C., Chiew, J., Rodriguez, D. L., Ting, E., and Lebofsky, S., “Wind Tunnel Investigation of a Flexible Wing High-Lift Configuration with a Variable Camber Continuous Trailing Edge Flap Design,” *AIAA Aviation Forum*, 2015. https://doi.org/https://doi.org/10.2514/6.2015-2417.

[13] Precup, N., Mor, M., and Livne, E., “An Active Variable Camber Continuous Trailing Edge Flapped Wing Wind Tunnel Model for Aeroelastic "In-Flight" Shape Optimization Tests,” *AIAA Aviation Forum*, 2018. https://doi.org/https://doi.org/10.2514/6.2018-3106.

[14] Nguyen, N. T., Cramer, N. B., Hashemi, K. E., Drew, M. C., Xiong, J., Mundt, T., Mor, M., and Livne, E., “Progress on Gust Load Alleviation Wind Tunnel Experiment and Aeroservoelastic Model Validation for a Flexible Wing with Variable Camber Continuous Trailing Edge Flap System,” *AIAA SciTech Forum*, 2020. https://doi.org/https://doi.org/10.2514/6.2020-0214.

[15] Berg, J., Ting, K.-Y., Mor, M., and Livne, E., “Analysis Active Control Exploration using the University of Washington’s Multiple Control Surface Large Flexible Wing,” *AIAA SciTech Forum*, 2025. https://doi.org/https://doi.org/10.2514/6.2025-1854.

[16] Berg, J., Ting, K.-Y., Mundt, T. J., Mor, M., Livne, E., and Morgansen, K. A., “Exploratory Wind Tunnel Gust Alleviation Tests of a Multiple-Flap Flexible Wing,” *AIAA SciTech Forum*, 2021. https://doi.org/https://doi.org/10.2514/6.2022-2488.

[17] Quenzer, J. D., Zongolowicz, A., Hinson, K. A., Barzgaran, B., Livne, E., Mesbahi, M., and Morgansen, K., “Model for Aeroelastic Response to Gust Excitation,” *AIAA SciTech Forum*, 2019. https://doi.org/https://doi.org/10.2514/6.2019-2031.

[18] Nguyen, N. T., “Hamiltonian Adaptive and Optimal Control of Lagrangian Infinite-Dimensional Systems with Gust Load Alleviation Application,” *AIAA SciTech Forum*, 2021. https://doi.org/https://doi.org/10.2514/6.2021-1129.

[19] Nguyen, N. T., Hashemi, K. E., Arabi, E., and Yucelen, T., “Model-Reference Adaptive Control of Distributed Lagrangian Infinite-Dimensional Systems Using Hamilton’s Principle,” *AIAA SciTech Forum*, 2020. https://doi.org/https://doi.org/10.2514/6.2020-0840.

[20] Nguyen, N. T., “Distributed Optimal Control of Lagrangian Infinite-Dimensional Systems with Kalman Filter Estimation,” *AIAA SciTech Forum*, 2022. https://doi.org/https://doi.org/10.2514/6.2022-2027.

[21] Nguyen, N. T., “Distributed Optimal Control and Estimation of Lagrangian Infinite-Dimensional Systems Coupled to Finite-Dimensional Systems,” *AIAA SciTech Forum*, 2023. https://doi.org/https://doi.org/10.2514/6.2023-1633.

[22] Nguyen, N. T., and Tuzcu, I., "Nonlinear Distributed Hamiltonian Control of Very Flexible Aircraft with Adaptive Gust Rejection," *AIAA SciTech Forum*, 2024. https://doi.org/https://doi.org/10.2514/6.2024-1784.

[23] Nguyen, N. T., "Distributed Hamiltonian Adaptive Disturbance Rejection Control With Actuator Dynamics," *AIAA SciTech Forum*, 2025. https://doi.org/https://doi.org/10.2514/6.2025-2801.